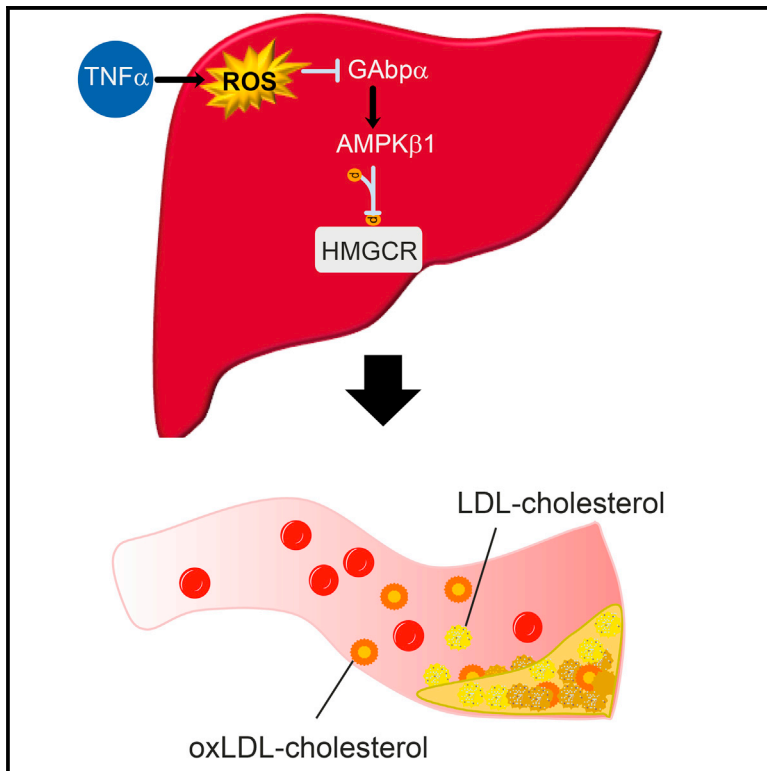# Cell Reports

A Hepatic GAbp-AMPK Axis Links Inflammatory Signaling to Systemic Vascular Damage

Graphical Abstract

Authors

Katharina Niopek, Bilgen Ekim Üstünel, Susanne Seitz, ..., Anja Zeigerer, Stephan Herzig, Mauricio Berriel Diaz

Correspondence

stephan.herzig@helmholtz-muenchen.de (S.H.),
mauricio.berrieldiaz@helmholtz-muenchen.de (M.B.D.)

In Brief

Inflammatory signaling contributes to metabolic disease progression in obesity and diabetes. Niopek et al. identify the transcription factor GAbp to be inactivated in the liver by TNF-α-dependent oxidative stress. Inactivation of GAbp increases cholesterol levels through impaired hepatic AMPK function, contributing to macro-vascular lesion formation as a diabetic long-term complication.

Highlights

- TNF-α-induced ROS formation diminishes hepatic GAbp transcription factor function

- Impaired hepatic GAbp function results in transcriptional inactivation of AMPK

- AMPK deficiency increases hepatic cholesterol secretion

- Hypercholesterolemia upon GAbp inhibition induces atherosclerotic lesion formation

Accession Numbers

E-MTAB-5775
E-MTAB-5831

CrossMark

CellPress

A Hepatic GAbp-AMPK Axis Links Inflammatory Signaling to Systemic Vascular Damage

Katharina Niopek,[1,2] Bilgen Ekim Üstünel,[1,2] Susanne Seitz,[1,2] Minako Sakurai,[1,2] Annika Zota,[1,2] Frits Mattijssen,[1,2] Xiaoyue Wang,[3] Tjeerd Sijmonsma,[3] Yvonne Feuchter,[3] Anna M. Gail,[3] Barbara Leuchs,[4] Dominik Niopek,[5,6] Oskar Staufer,[1,2] Maik Brune,[1,2] Carsten Sticht,[7] Norbert Gretz,[7] Karin Müller-Decker,[8] Hans-Peter Hammes,[9] Peter Nawroth,[1,2,10] Thomas Fleming,[10] Michael D. Conkright,[11] Matthias Blüher,[12] Anja Zeigerer,[1,2] Stephan Herzig,[1,2,13,*] and Mauricio Berriel Diaz[1,2,*]

[1]Institute for Diabetes and Cancer (IDC), Helmholtz Center Munich and Technical University Munich, 85764 Neuherberg, Germany
[2]Joint Heidelberg-IDC Translational Diabetes Program, Inner Medicine 1, Heidelberg University Hospital, 69120 Heidelberg, Germany
[3]Joint Division Molecular Metabolic Control, DKFZ-ZMBH Alliance and Network Aging Research, German Cancer Research Center, 69120 Heidelberg, Germany
[4]Division of Tumor Virology, German Cancer Research Center, 69120 Heidelberg, Germany
[5]Division of Theoretical Bioinformatics (B080), German Cancer Research Center, 69120 Heidelberg, Germany
[6]Department of Bioinformatics and Functional Genomics, Institute for Pharmacy and Biotechnology and BioQuant, University of Heidelberg, 69120 Heidelberg, Germany
[7]Medical Research Center, Klinikum Mannheim, 68167 Mannheim, Germany
[8]Core Facility Tumor Models, German Cancer Research Center, 69120 Heidelberg, Germany
[9]5th Medical Department, University Medicine Mannheim, University of Heidelberg, 68167 Mannheim, Germany
[10]Department of Internal Medicine I and Clinical Chemistry, University of Heidelberg, 69120 Heidelberg, Germany
[11]Department of Cancer Biology, The Scripps Research Institute, Jupiter, FL 33458, USA
[12]Department of Medicine, University of Leipzig, 04103 Leipzig, Germany
[13]Lead Contact
*Correspondence: stephan.herzig@helmholtz-muenchen.de (S.H.), mauricio.berrieldiaz@helmholtz-muenchen.de (M.B.D.)
http://dx.doi.org/10.1016/j.celrep.2017.07.023

SUMMARY

Increased pro-inflammatory signaling is a hallmark of metabolic dysfunction in obesity and diabetes. Although both inflammatory and energy substrate handling processes represent critical layers of metabolic control, their molecular integration sites remain largely unknown. Here, we identify the heterodimerization interface between the α and β subunits of transcription factor GA-binding protein (GAbp) as a negative target of tumor necrosis factor alpha (TNF-α) signaling. TNF-α prevented GAbpα and β complex formation via reactive oxygen species (ROS), leading to the non-energy-dependent transcriptional inactivation of AMP-activated kinase (AMPK) β1, which was identified as a direct hepatic GAbp target. Impairment of AMPKβ1, in turn, elevated downstream cellular cholesterol biosynthesis, and hepatocyte-specific ablation of GAbpα induced systemic hypercholesterolemia and early macro-vascular lesion formation in mice. As GAbpα and AMPKβ1 levels were also found to correlate in obese human patients, the ROS-GAbp-AMPK pathway may represent a key component of a hepato-vascular axis in diabetic long-term complications.

INTRODUCTION

Pro-inflammatory cytokines have been causally linked to acute immunological reactions such as septic shock, as well as to the low-grade, chronic inflammatory state associated with obesity and the metabolic syndrome (Gregor and Hotamisligil, 2011; Shoelson et al., 2007).

Indeed, metabolic disease conditions are characterized by elevated levels of interleukins (ILs) 1β and 6 and tumor necrosis factor alpha (TNF-α) (Alexandraki et al., 2006; Miyazaki et al., 2003). Ablation of the TNF-α gene or of its receptor protects mice from the development of insulin resistance and associated metabolic disorders (Uysal et al., 1997, 1998), while chronic exposure of mice to TNF-α is sufficient to cause a cachectic and insulin resistance phenotype in mice (Akram, 2013; Oliff et al., 1987).

In addition to the impairment of endocrine circuits, metabolic dysfunction is typically characterized by faulty cellular energy sensing, leading to aberrant systemic energy homeostasis. Under physiological conditions, the AMP-activated protein kinase (AMPK) complex responds to a low cellular energy (i.e., ATP) status by switching from anabolism to catabolism (Hardie, 2014). Defective AMPK-mediated energy sensing, coupled to mal-adaptation of energy substrate handling, has thus been identified as a key event in metabolic dysfunction (Coughlan et al., 2014). Furthermore, AMPK activation has been found to counteract inflammatory processes (O'Neill and Hardie, 2013), further supporting a tight correlation between inflammatory signaling and dysfunctional energy sensing in chronic metabolic disease conditions. However, how pro-inflammatory cytokine signaling affects cellular energy sensing complexes remains largely unknown.

Here, we identify the heterodimerization between GA-binding protein (GAbp) subunits α and β as a critical target of TNF-α-dependent reactive oxygen species (ROS) formation. GAbpα was found to be an upstream regulator of AMPK, thereby
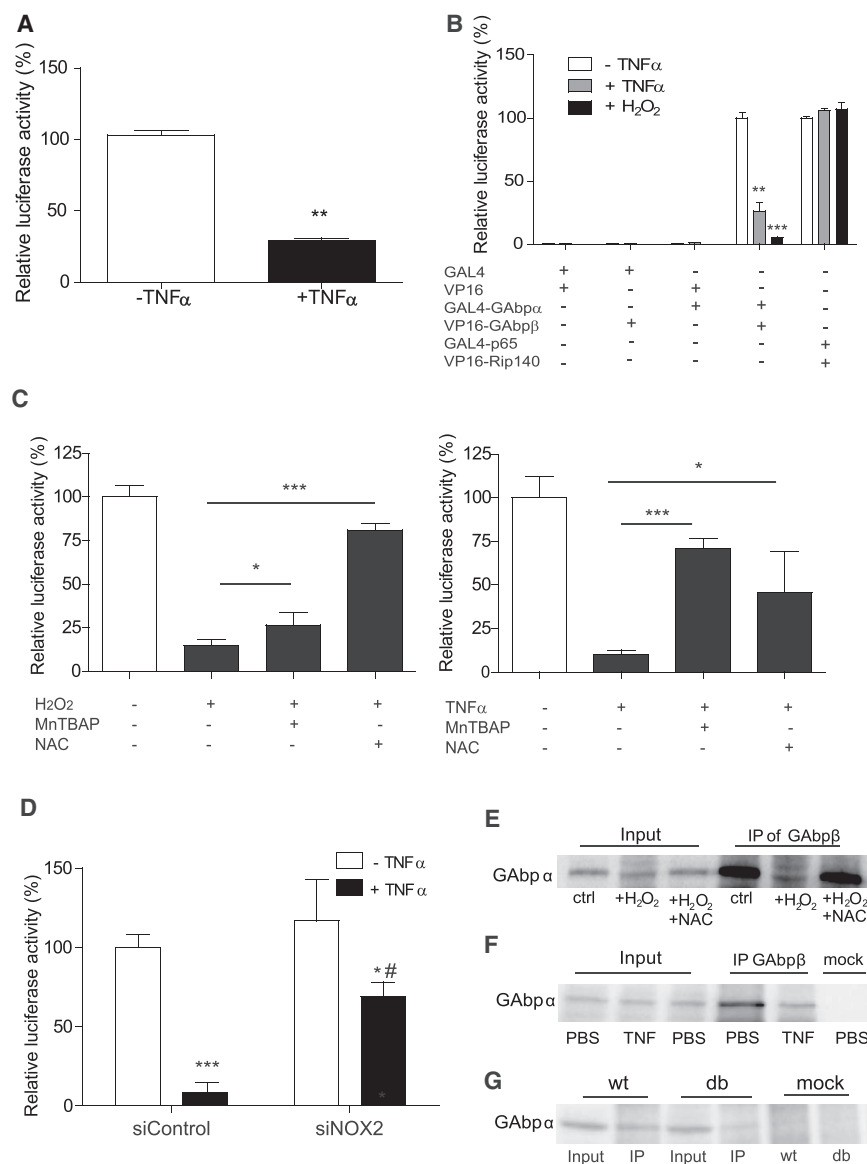
CrossMark

Figure 1. TNF-α Disrupts GAbp Transcriptional Complex Formation via Reactive Oxygen Species

(A) Mammalian one-hybrid assay showing alteration of relative luciferase activity of Gal4-GAbpα upon TNF-α stimulation. HEK293T cells were transfected with Gal4-luc, pCMV-β-gal, and Gal4-GAbpα and stimulated 24 hr with 100 ng/mL TNF-α. Relative luciferase activity was normalized to untreated (vehicle) control (data are mean ± SEM; **p ≤ 0.01; n = 6).

(B) Mammalian two-hybrid assay in Hepa1-6 cells. Cells were transfected with Gal4-luc, pCMV-β-gal, and GAL4-DNA binding domain (GAL4), GAL4-DBD-GABPα, or GAL4-DBD-p65, together with pCMX-VP16, pCMX-VP16-GABPβ1, or pCMX-VP16-Rip140 treated with 20 ng/mL TNF-α and 500 μM H_2O_2 as indicated (data are mean ± SEM relative to untreated control; **p ≤ 0.01, ***p ≤ 0.001; n = 6).

(C) Mammalian two-hybrid assay in Hepa1-6 cells treated with 20 ng/mL TNF-α and 500 μM H_2O_2 and 5 mM N-acetylcysteine (NAC) or 150 μM MnTBAP as indicated (data are mean ± SEM; **p ≤ 0.01, ***p ≤ 0.001; n = 3).

(D) Mammalian two-hybrid assay in Hepa1-6 cells treated with 20 ng/mL TNF-α and siRNA against Nox2 as indicated (data are mean ± SEM; #p ≤ 0.05 siControl versus siNOX2, *p ≤ 0.05 –TNF-α versus +TNF-α; n = 3).

(E) Immunoprecipitation (IP) of GAbpβ and blot for GAbpα in primary hepatocytes treated with vehicle (ctrl) or 500 μM H_2O_2 or 500 μM H_2O_2 and 5 mM NAC, respectively. GAbpα was measured in 5% input as loading control.

(F) IP of GAbpβ and blot for GAbpα from liver of wild-type mice treated with vehicle or 5 μg/kg recombinant TNF-α. GAbpα was measured in 5% input as loading control.

(G) IP of GAbpβ and blot for GAbpα from liver of wild-type and db/db mice. IgG was used for pull-down as mock IP. GAbpα was measured in 5% input as loading control.

See also Figure S1.

controlling cellular and systemic cholesterol homeostasis as well as early vascular lesion formation in vivo.

RESULTS

TNF-α Induces ROS-Mediated Dissociation of the GAbp Complex

To identify transcriptional regulators implicated in intra-cellular pro-inflammatory signaling, we used a GAL4 one-hybrid plasmid library as previously described (Amelio et al., 2007). The library was co-transfected with a GAL4-responsive luciferase reporter into human embryonic kidney (HEK) cells, and cells were treated with TNF-α or vehicle (Figure S1A). Putative TNF-α targets from the screen were validated in a subsequent manual screening. Among the proteins most robustly repressed in their activity by

TNF-α was the transcription factor GAbpα (Figure 1A). GAbpα is a member of E26 transformation-specific (Ets) transcription factors and binds to DNA sequences rich in guanine and adenine. The subunit GAbpα itself has a DNA binding domain with a winged-helix-turn-helix motif but needs to interact with the partner protein GAbpβ to form a transcriptionally active heterotetramer (Rosmarin et al., 2004).

GAbpα is strongly expressed in the liver, and importantly, metabolic dysfunction in this organ represents a key feature of various inflammation-associated pathologies, including obesity, insulin resistance and non-alcoholic fatty liver disease (NAFLD) (Cai et al., 2005; Michael et al., 2000; Turner et al., 2013). Therefore, we aimed to further explore the importance of TNF-α-dependent control of GAbpα activity specifically in the hepatic context.

Given that GAbpα lacks an intrinsic transactivation domain (Batchelor et al., 1998), we tested whether the reduced GAbpα transactivation in response to TNF-α treatment was due to impaired GAbpβ recruitment. To this end, we used a mammalian two-hybrid interaction assay using GAbpα fused to the GAL4 DNA binding domain (GAL4-DBD-GAbpα) and GAbpβ to the VP16-transactivation domain (VP16-GAbpβ), which allows monitoring the mere interaction of the two subunits in response to a stimulus independent of intrinsic DNA-binding and transactivation functions of GAbpα and GAbpβ. As expected, both GAbp subunits showed a strong interaction upon co-transfection alongside with a GAL4-luc reporter into the murine hepatoma cell line Hepa1-6, while negative controls containing only a GAL4 DNA binding domain or a VP16 transactivation domain did not result in appreciable transactivation (GAL4-DBD and pCMX-VP16, respectively) (Figure 1B).

TNF-α treatment reduced the GAbpα/β interaction by about 4-fold (Figure 1B), while not affecting protein expression of the transfected fusion constructs (Figure S1B), and promoted GAbp complex dissociation in a dose-dependent manner (Figure S1C).

TNF-α has previously been shown to trigger the generation of ROS (Houstis et al., 2006). Interestingly, GAbpα harbors redox-sensitive cysteine residues within its minimal GAbpβ binding domain (Chinenov et al., 1998; Martin et al., 1996), suggesting that TNF-α may control GAbp complex formation through ROS-dependent mechanisms. In line with this hypothesis, we observed a strong inhibition of GAbpα/β interaction upon treatment of hepatoma cells with hydrogen peroxide (H_2O_2) (Figure 1B). Importantly, unrelated protein-protein interactions (Zschiedrich et al., 2008) remained independent of TNF-α or ROS stimulation (Figure 1B). Furthermore, increasing H_2O_2 concentrations revealed a dose-dependent dissociation of the GAbp complex (Figure S1D).

Further substantiating the notion that TNF-α signaling controls GAbp complex formation via intra-cellular ROS, the observed impaired interaction between GAbpα and GAbpβ in response to both TNF-α as well as H_2O_2 treatment was efficiently rescued by concomitant treatment with distinct ROS scavengers, N-acetylcysteine (NAC) or Mn(III)tetrakis(4-benzoic acid) porphyrin chloride (MnTBAP) (Figure 1C).

TNF-α signaling has been shown to induce ROS production through activation of the NADPH oxidase 2 (Nox2) (Li et al., 2009). Consequently, we applied a combination of TNF-α treatment and small interfering RNA (siRNA)-mediated knockdown of Nox2 to the GAbp two-hybrid interaction assay, which strongly abolished the TNF-α-induced dissociation of the GAbp complex (Figure 1D), indicating the involvement of Nox2-dependent ROS production in this process.

To ascertain whether the ROS-dependent GAbp complex dissociation can also be observed in non-immortilized cells, we treated primary mouse hepatocytes with H_2O_2 and analyzed the interaction of the endogenous GAbp subunits by co-immunoprecipitation (co-IP). Although treatment with H_2O_2 blocked the interaction between the endogenous subunits of the complex, concomitant treatment with NAC rescued the interaction (Figure 1E). These results further consolidate the findings from the two-hybrid assays by demonstrating that also the

endogenous GAbp complex is subject to regulation by ROS such as H_2O_2.

To corroborate these results in an in vivo setting, we next injected mice with TNF-α, thereby inducing hepatic inflammation (Geier et al., 2005). The mice were sacrificed when still exhibiting elevated circulating TNF-α levels (Figure S1E), and livers were subjected to co-IP as described above. In congruence with the results in primary hepatocytes, intraperitoneal (i.p.) TNF-α administration resulted in GAbpα/β complex dissociation (Figure 1F).

To verify whether the GAbp complex assembly is similarly perturbed in the liver of a disease model that intrinsically exhibits increased levels of TNF-α and oxidative stress (Mariappan et al., 2010; Yamakawa et al., 1995), we conducted a co-IP in wild-type and db/db mice. The latter is a model for obesity and type 2 diabetes characterized by increased blood sugar levels, dyslipidemia, and elevated hepatic TNF-α levels (Figure S1F) (Panchal and Brown, 2011). The co-IP indicated a dissociation of the GAbpα/β complex in livers of the db/db mice in contrast to evident GAbpα/β interaction in livers from controls (Figure 1G).

Taken together, our data suggest that the hepatic GAbp complex represents a molecular target of cytokine signaling via redox-sensitive dissociation of its subunits.

Liver-Specific Inhibition of GAbpα Induces Hypercholesterolemic Dyslipidemia

To study the physiological impact of impaired hepatic GAbp function in vivo, we knocked down GAbpα specifically in parenchymal liver cells using a hepatocyte-specific adeno-associated virus (AAV) microRNA (miRNA) delivery system in both wild-type and obese db/db mice (Kulozik et al., 2011). Eight weeks post-injection, mice were sacrificed after a fasting or a fasting-refeeding cycle (Figure 2A) in order to assess GAbp function under opposing physiological states. GAbpα knockdown was efficient on mRNA (Figure S2A) and protein level (Figure 2B). Concurrently, GAbpβ mRNA expression was induced upon GAbpα knockdown.

Interestingly, knockdown resulted in increased circulating cholesterol levels (Figure 2C), which was observed in all conditions. Increased cholesterol levels were allocated to low-density lipoprotein (LDL) as well as high-density lipoprotein (HDL) particles (Figure 2D). Interestingly, LDL cholesterol, which is associated with increased cardiovascular disease risk, was particularly elevated in db/db mice.

Other metabolic serum and liver parameters were either unchanged after hepatic GAbpα loss of function or affected only under specific physiological conditions, such as fasting (Figure S2B). Oil Red O staining for neutral lipids in liver tissue corroborated the finding of increased lipids in fasted db/db mice (Figure S2C). Interestingly, knockdown of GAbpα was associated with a significant elevation in liver lipid peroxidation (Figure S2D), suggesting increased oxidative stress.

In sum, the experiment revealed a critical role of the hepatic GAbp complex in cholesterol homeostasis. Also of note, GAbpα/β complex dissociation by acute TNF-α injection (Figure 1F) correlated with elevated serum cholesterol levels compared with controls (Figure S3B), thus supporting a mechanistic axis between GAbp action and hepatic cholesterol homeostasis.
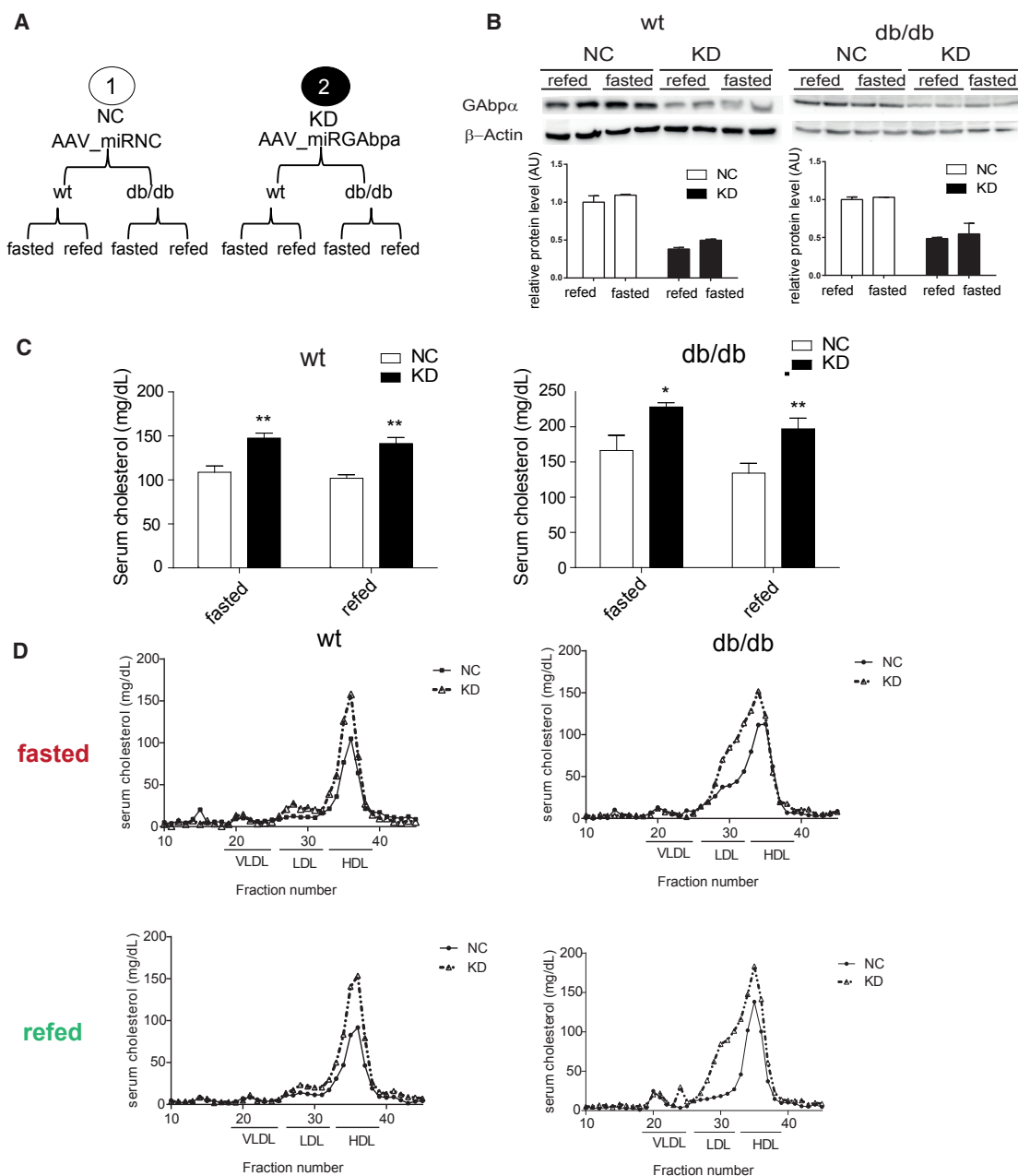
Figure 2. Hepatocyte-Specific GAbpα Knockdown Disrupts Lipostasis through Diminished AMPK Signaling

(A) Overview of the experimental groups used for hepatocyte-specific GAbpα knockdown in wild-type (wt) and db/db mice (Kulozik et al., 2011).

(B) Immunoblots and corresponding densitometric analysis for GAbpα in liver protein lysates from wild-type and db/db mice treated with AAV-miRNC (NC) or AAV-miRGAbpα (KD). Actin was used as loading control.

(C) Changes in total serum cholesterol in wild-type and db/db mice upon hepatic GAbpα knockdown (data are mean ± SEM; **p ≤ 0.01; n = 5).

(D) Distribution of serum cholesterol in different lipoprotein fractions measured by fast-liquid protein chromatography (FPLC).

See also Figure S2.

Knockdown of Hepatic GAbpα Diminishes AMPK Function

To determine changes in the transcriptome that might account for the phenotypic observations, we performed mRNA expression profiling. All eight AAV-injected experimental groups as depicted in Figure 2A were included in the analysis, in which direct comparison of gene expression was performed separately between corresponding negative control (NC) and GAbpα knockdown samples for the different conditions (wild-type or db/db; fasting or refeeding). Notably, we found the largest number of differentially expressed genes in fasted wild-type mice, in agreement with more phenotypic changes in serum and liver lipid

levels (Figure S2B). The markedly reduced number of differentially expressed genes upon GAbpα knockdown in db/db mice compared with wild-type mice (Figure 3A) was potentially due to already diminished GAbp complex stability under metabolic disease conditions (Figure 1G).

Among the genes that we found consistently downregulated upon knockdown of GAbpα in fasting as well as refeeding states was the 5′AMP-activated protein kinase b1. AMPKβ1 is the regulatory subunit of the AMPK heterotrimer, which represents the principle cellular energy sensor (Hardie, 2014). Indeed, we could confirm that AMPKβ1 was downregulated in GAbpα knockdown livers (Figure 3B), while also TNF-α treatment of wild-type mice inhibited AMPKβ1 and α protein expression, correlating with elevated cholesterol levels (Figures S3A and S3B). This was particularly interesting, because AMPK regulates cholesterol biosynthesis via inhibitory phosphorylation of the rate-limiting enzyme 3-hydroxy-3-methyl-glutaryl-CoA reductase (HMGCoAR) (Corton and Hardie, 1996; Motoshima et al., 2006), thereby providing a possible explanation for the increased circulating cholesterol levels in hepatic GAbpα deficient mice. We could show that diminished GAbpα protein levels in knockdown livers were associated with strong reductions in both protein levels of AMPKβ1 and the inactive phosphorylated form of HMGCoAR (Figure 3C). Similarly, we found reduced levels of phosphorylated sterol regulatory element-binding protein (SREBP) 1c (Figure 3C), representing a central regulator of lipid metabolism. Intriguingly, SREBP1c was also identified as target of inhibitory phosphorylation by AMPK, a mechanism that was described to attenuate hepatic steatosis and atherosclerosis (Li et al., 2011). Of note, total protein levels of HMGCoAR and SREBP1c remained unchanged (Figure S3C). Interestingly, AMPKα and AMPKγ protein levels were also reduced in knockdown samples (Figure 3C). It was shown by Qi et al. (2008) that the AMPK subunits become instable when the stoichiometry of the three different subunits is disturbed. Congruently, we found that hepatic AMPK activity was indeed lower upon GAbpα knockdown as determined by AMPK kinase activity assay (Figures 3D and 3E).

The phosphorylation of the AMPK targets SREBP1c, HMGCoAR, and ACC was diminished in relation to total protein (Figures 3C and S3D). In addition, reduced phosphorylation of ACC was observed in cells upon knockdown of GAbpα in the absence or presence of stimulation with the AMPK activator AICAR (Figure S3E). Also, treatment of primary mouse hepatocytes with increasing amounts of H_2O_2 led to a dose-dependent loss of AMPKα and β expression, correlating with reduced ACC phosphorylation (Figure S3F).

In agreement with the in vivo phenotype, knockdown of GAbpα in primary mouse hepatocytes resulted in accumulation of cholesterol in the medium (Figure 3F). Remarkably, this effect was rescued by concomitant HMGCoAR inhibition with simvastatin, indicating its central role in the GAbpα pathway. In a similar approach, we found that the increased cholesterol secretion by primary hepatocytes upon GAbpα knockdown was also rescued through reconstitution of AMPK function by overexpressing a constitutively active form of AMPKα1 (Prkaa1^{T172D}) (Figure 3G), indicating that AMPK is indeed the main mediator of induced cholesterol synthesis upon GAbp loss of function.

To determine genomic sites of direct GAbpα recruitment in liver tissue, we performed chromatin immunoprecipitation followed by DNA sequencing (ChIP-seq). We found a marked enrichment of DNA sequences in immediate proximity to the AMPKβ1 transcriptional start site (Figure 3H), indicating direct recruitment of GAbpα.

To validate a direct role of GAbp for AMPK transcriptional control, we used promoter activation assays and found that GAbpα/β overexpression significantly enhanced AMPKβ1 promoter activity, while H_2O_2 or TNF-α treatment reversed this effect (Figure 3I).

In line with the previous findings, GAbpα levels positively correlated with mRNA levels of AMPKβ1 in both male and female obese human patients (Figure 3J), indicating that elevated GAbpα activity is indeed coupled to enhanced AMPKβ1 transcript levels also in the human setting.

Loss of Hepatic GAbpα Function Induces Early Markers of Atherogenesis

Given the hypercholesterolemia upon knockdown of hepatic GAbpα, we next sought to investigate GAbpα function in macro-vascular complications as associated with metabolic diseases (Kalofoutis et al., 2007). To this end, we used male LDL receptor knockout (LDLR-KO) mice, which are prone to atherosclerosis development if exposed to triggers such as a high-cholesterol diet or type 1 diabetes (Ishibashi et al., 1994; Vikramadithyan et al., 2005).

As before, knockdown of hepatic GAbpα was achieved by injection of AAVs. In addition, experimental groups were analyzed in the presence or absence of streptozotocin (STZ)-induced type 1 diabetes. STZ treatment was previously shown to promote atherosclerosis development in LDLR-KO mice and served as a reference treatment to assess atherogenic lesion formation (Keren et al., 2000; Kunjathoor et al., 1996; Mathé, 1995; Vikramadithyan et al., 2005), enabling us to gauge the capacity of GAbpα knockdown to initiate lesion formation, as well as for the combination of both treatments. Furthermore, to analyze the impact of dietary cholesterol supplementation on atherosclerosis development, for all experimental conditions described above, the mice were fed either a normal chow diet or a 0.15% high-cholesterol diet. A schematic overview of experimental groups is depicted in Figure 4A.

Knockdown of GAbpα in livers of LDLR-KO mice was confirmed on mRNA (Figure S4A) as well as protein level (Figure 4B). Immunohistochemistry with a GAbpα-specific antibody showed no change in GAbpα level in aortic endothelial cells (Figure S4B). As before, knockdown of hepatic GAbpα in LDLR-KO mice increased serum cholesterol levels (Figure 4C). The effect of diminished GAbpα expression on circulating cholesterol was comparable with the elevated levels due to STZ-induced diabetes (Figure 4C), the latter of which have been described before (Goldberg et al., 2008; Keren et al., 2000; Vikramadithyan et al., 2005).

In general, induced hypercholesterolemia upon knockdown or STZ-induced diabetes was observed under both dietary conditions but at an overall higher level in mice fed a high-cholesterol diet (Figure 4C). LDL cholesterol levels were increased by knockdown of hepatic GAbpα (Figure 4D). STZ-induced diabetes in
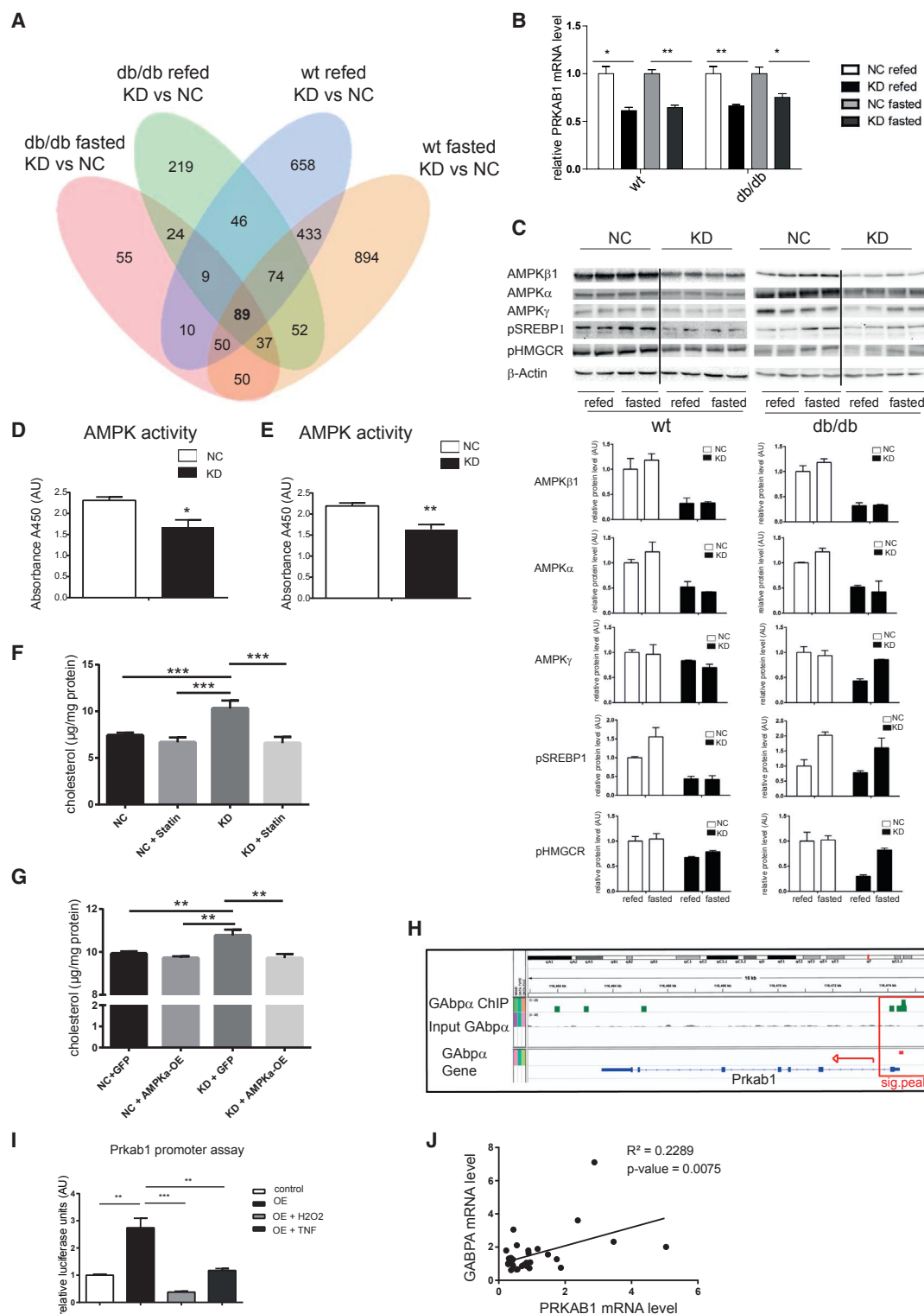
Figure 3. GAbp Controls the AMPK Signaling Pathway

(A) Venn diagram showing the overlap of differentially expressed genes in the transcriptome profiling of fasted and refed wild-type and db/db mice upon hepatic GAbpα knockdown (n = 3).

(B) mRNA levels of 5′AMP-activated protein kinase beta-1 subunit (AMPKβ1/ prkab1) during fasting and refeeding in wt and db/db mice upon hepatic GAbpα knockdown (data are mean ± SEM; *p ≤ 0.05, **p ≤ 0.01; n = 4 or 5).

(legend continued on next page)

chow diet-fed mice resulted in additionally increased cholesterol loading into very low-density lipoprotein (VLDL) particles, which was synergistically enhanced when combined with GAbpα knockdown (Figure 4D). As expected, high-cholesterol diet feeding led to very high basal levels of VLDL and LDL cholesterol, which were moderately further increased by STZ-induced diabetes or GAbpα knockdown (Figure 4D).

Other serum parameters were either unchanged after hepatic GAbpα loss of function in LDLR-KO mice or affected only under specific treatment conditions (Figures S4C–S4E). Furthermore, liver lipids were increased in the analyzed conditions to different extents (Figures S4F and S4G). The observed effects on hepatic lipid levels determined by enzymatic assays were also reflected in Oil Red O staining of liver sections (Figure 4E).

Finally, we evaluated atherogenic precursor lesion formation within the entire aorta. Representative images of aortic arches and diverging blood vessels as well as corresponding quantifications of early fatty streak areas are shown for the main comparison of NC and GAbpα knockdown non-diabetic mice (Figure 4E) and in Figure S4I including STZ-induced diabetic mice. In chow diet-fed, non-diabetic NC mice, the aortas were almost devoid of fatty streaks (Figure 4E). Diminished hepatic GAbpα expression alone was sufficient to induce a 4-fold increase in fatty streaks (Figure 4E). Similarly, STZ-induced diabetes alone induced aortic lipid accumulation to the same extend (Figure S4I), correlating with comparable effects on serum cholesterol levels (Figure 4C). As expected, high-cholesterol diet feeding strongly increased lesion area (Figure 4E). Notably, also high-cholesterol diet-induced fatty streak formation was further aggravated by concurrent knockdown of hepatic GAbpα (Figure 4E). As observed before for serum cholesterol levels, combined GAbpα knockdown and STZ-induced diabetes under chow diet-fed conditions resulted in a 9-fold increase in fatty streak formation (Figure S4I). However, we did not find such synergistic effects in the combined treatment group on high-cholesterol diet (Figure S4I). In sum, hepatic GAbpα knockdown caused early atherosclerotic lesion formation in a way that closely correlated with corresponding effects on serum cholesterol levels and the formation of atherogenic oxidized LDL (oxLDL) particles (Figure 5A). Also, diminished hepatic GAbpα levels were again associated with reduced AMPK signaling (Figures 5B, S5A, and S5B).

In line with diminished phosphorylation of SREBP1c by AMPK at Ser372, hepatic mRNA expression of the SREBP targets fatty acid synthase (FASN) and HMGCoAR were upregulated upon GAbpα knockdown in cholesterol diet-fed LDLR-KO mice with similar tendencies for stearoyl-CoA desaturase-1 (SCD-1) and ACC (Figure S5C). In chow-fed LDLR-KO mice, hepatic knockdown of GAbpα tended to upregulate SCD-1 and HMGCoAR mRNA, while FASN and ACC expression was unaffected (Figure S5C).

Of note, in human patients, hepatic GAbpα levels positively correlated with enhanced insulin sensitivity as determined by hyperinsulinemic-euglycemic clamps in obese patients (Figure 5C), suggesting that also in humans impaired GAbpα activity in liver associates with less favorable metabolic conditions that are linked to long-term complications including vascular damage.

DISCUSSION

In the present study, we provide in vitro and in vivo data showing that TNF-α-dependent ROS formation leads to the dissociation of the GAbp transcription factor complex in hepatocytes. In previous studies, DNA binding of GAbp was shown to be inhibited by pro-oxidant conditions in 3T3 cells (Martin et al., 1996) and in vitro DNA binding assays (Chinenov et al., 1998). However, our in vitro and in vivo data indicate that TNF-α/ROS-dependent control of GAbp activity is mediated via the ROS-sensitive GAbpα/β interaction surface as a major regulatory site, suggesting that GAbpα/β heterodimerization is a prerequisite for the active tetrameric complex formation, which in turn might also require DNA binding (Chinenov et al., 2000).

Similarly, another study has identified threonine 280 as a specific phosphorylation site required for the transcriptional activation of GAbp in vitro and in vivo (Fromm and Burden, 2001). Although GAbp phosphorylation and activation have been shown to be mediated through ERK and JNK MAP kinase pathways in NRG-stimulated muscle cells (Fromm and Burden, 2001; Sunesen et al., 2003), oxidative modifications of distinct cysteine residues or other redox-dependent mechanisms are now suggested to confer transcriptional inhibition.

As yet, liver-specific functions of GAbp are only marginally understood. In two studies, the integration of global chromatin

(C) Immunoblots and corresponding densitometric analysis for AMPK pathway components in liver protein lysates from wild-type and db/db mice treated with AAV-miRNC (NC) or AAV-miRGAbpα (KD). Actin was used as loading control.

(D) AMPK activity assay in liver of wild-type mice treated with AAV-miRNC (NC) or AAV-miRGAbpα (KD). AMPK was measured as phosphorylation of IRS1 S789 with the CycLex AMPK kinase assay kit (data are mean ± SEM; **p ≤ 0.01; n = 5).

(E) AMPK activity assay in liver of db/db mice treated with AAV-miRNC (NC) or AAV-miRGAbpα (KD) (data are mean ± SEM; **p ≤ 0.01; n = 5).

(F) Cholesterol production by control and GAbpα knockdown hepatocytes treated with DMSO or 50 μM simvastatin for 5 hr measured in serum-free medium as micrograms per milligram cellular protein (mean ± SEM; **p < 0.01; n = 9–12).

(G) Cholesterol production by hepatocytes transfected with control or GAbpα-specific siRNA with concomitant overexpression of GFP or a constitutively active form (Prkaa1^{T172D}) of AMPKα1 (Ampkα1-OE) measured after 5 hr in serum-free medium as micrograms per milligram cellular protein (mean ± SEM; **p < 0.01; n = 6).

(H) Cistrome analysis of GAbpα binding sites in the prkab1 gene in wild-type mice. The significantly enriched peaks are shown in green, and the gene promoter is marked in red.

(I) Reporter assay in HEK293T cells with the prkab1 promoter in the presence of overexpressed GAbpα/β treated with 20 ng/μl with TNF-α or 500 μM H$_2$O$_2$ or left untreated (data are mean ± SEM; *p ≤ 0.05 [relative to control OE construct], **p ≤ 0.01, ***p ≤ 0.001 [relative to untreated GAbpα/β overexpression]; n = 3).

(J) Correlation and p value shown for normalized GABPα versus AMPKB1 mRNA levels in livers of obese human subjects (n = 30; Pearson correlation coefficient = 0.478; p = 0.0075).
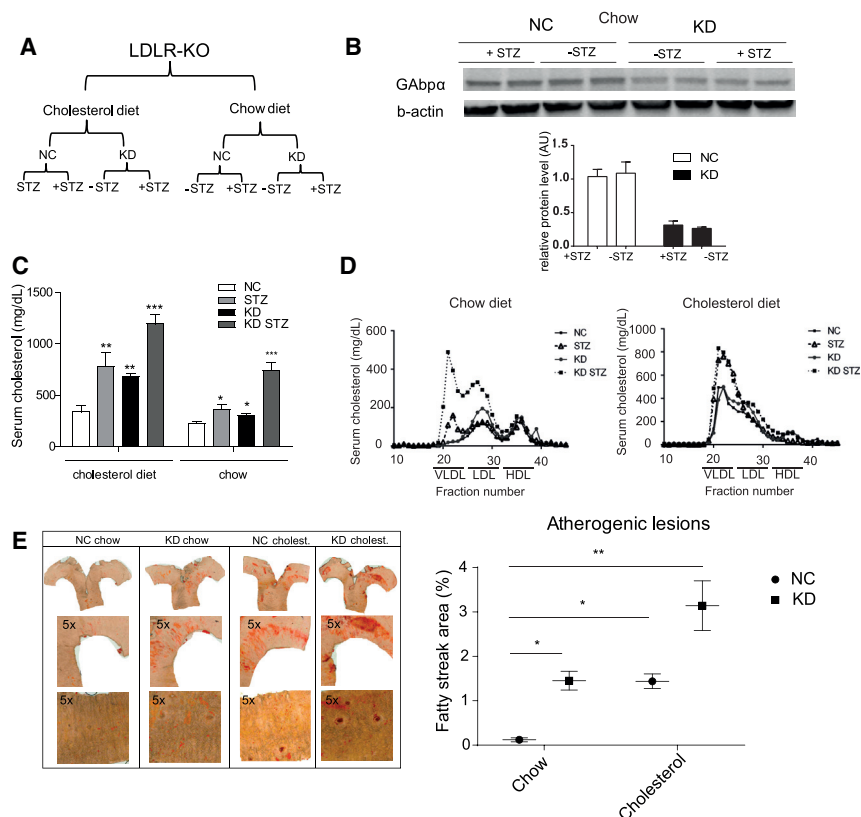
See also Figure S3.

Figure 4. GAbpα Knockdown Is Severely Atherogenic in LDLR-KO Mice

(A) Overview of the experimental groups used for hepatocyte-specific GAbpα knockdown in LDLR-KO mice.

(B) Immunoblot and corresponding densitometric analysis of GAbpα protein in chow-fed mouse liver upon hepatocyte-specific AAV-mediated GAbpα knockdown. Actin was used as loading control.

(C) Serum cholesterol in LDLR-KO mice upon hepatic GAbpα knockdown and STZ treatment when fed cholesterol or chow diet (data are mean ± SEM; *p ≤ 0.05, **p ≤ 0.01, ***p ≤ 0.001 [relative to NC]; n = 5).

(D) Distribution of serum cholesterol in different lipoprotein fractions measured by fast-liquid protein chromatography. Serum of five mice per group was pooled before fractionation (n = 5).

(E) Bright-field microscopy images of the aortic arch (upper image), 5× magnification of the aortic arch (middle image) and of vessels branching away from the aorta in chow and 0.15% cholesterol diet fed LDLR-KO mice treated with STZ or vehicle and control (NC) or GAbpα knockdown AAV (A, lower image). Quantification of aortic plaque area in paraffin-fixed aorta (data are mean ± SEM; *p ≤ 0.05, ***p ≤ 0.001; n = 5).

See also Figure S4.

recruitment patterns of individual transcription factors in human HepG2 hepatocytes suggested that GAbp cooperates with PGC1α (Charos et al., 2012) and HNF4 (Wallerman et al., 2009) in the transcriptional regulation of common subsets of target genes. However, functional downstream consequences were not described. Further, expression of the Yes-associated protein (YAP) gene in the liver was shown to be activated by GAbp, suggesting a role of GAbp in liver regeneration and carcinogenesis (Wu et al., 2013). In the same study, GAbp was shown to be inactivated by the Hippo pathway and, interestingly, also by oxidative stress (Wu et al., 2013), the latter of which is in agreement with our data, although in a different physiological context. Recently, the transactivation subunit GAbpβ1 was shown to be deacetylated by SIRT7 in the liver, thereby facilitating GAbp complex formation and suggesting a role in the regulation of nuclear encoded mitochondrial genes (Ryu et al., 2014). This study provides an additional mechanism for the regulation of GAbp by post-translational modification of the β subunit affecting complex formation.

Our data define a central role of the GAbp transcription factor in the maintenance of hepatic and systemic lipid homeostasis. Most prominently, hepatocyte-specific deficiency in GAbpα resulted in hypercholesterolemia, including increased levels of LDL cholesterol as an important component of atherogenic dyslipidemia in the metabolic syndrome (Chahil and Ginsberg, 2006; Klop et al., 2013). Indeed, indicating a protective role of GAbp function for early atherogenic lesion formation, depletion of

GAbpα expression in hepatocytes of LDLR-KO mice markedly increased lipid deposition (fatty streaks) in the aortas of these mice. Interestingly, GAbpα deficiency also increased the levels of both hepatic lipid peroxidation as well as circulating oxLDL levels, suggesting that in addition to the upstream oxidative inactivation of GAbp, impaired GAbp activity induces pro-oxidant conditions. Although further investigation is needed to decipher the exact mechanisms of GAbp-dependent anti-oxidant effects, it is tempting to speculate that it is associated with the role of GAbp in the regulation of OXPHOS genes and mitochondrial function (Rosmarin et al., 2004; Ryu et al., 2014) and/or in the regulation of the Hippo pathway (Wu et al., 2013).

AMPK activation is considered to exert a variety of beneficial metabolic effects, including amelioration of diabetic dyslipidemia and atherosclerosis (Li et al., 2011; Viollet et al., 2007). Also, the insulin-sensitizing effects of metformin are at least in part mediated by AMPK activation (Hardie, 2013). Furthermore, AMPK promotes ketogenesis (Viollet et al., 2009), which was not observed in the presented rather long-term in vivo experiments, possibly because of compensation by other β-oxidation regulatory mechanisms.

Previously, AMPK activation was shown to be induced by ROS in vitro in the context of hypoxia in muscle and cancer cells (Emerling et al., 2009; Mungai et al., 2011), a specific condition in which a metabolic switch is crucial to avoid energy deficiency and cell damage. Of note, hypoxia-induced AMPK activation was mediated by CAMKK2 function and was independent from
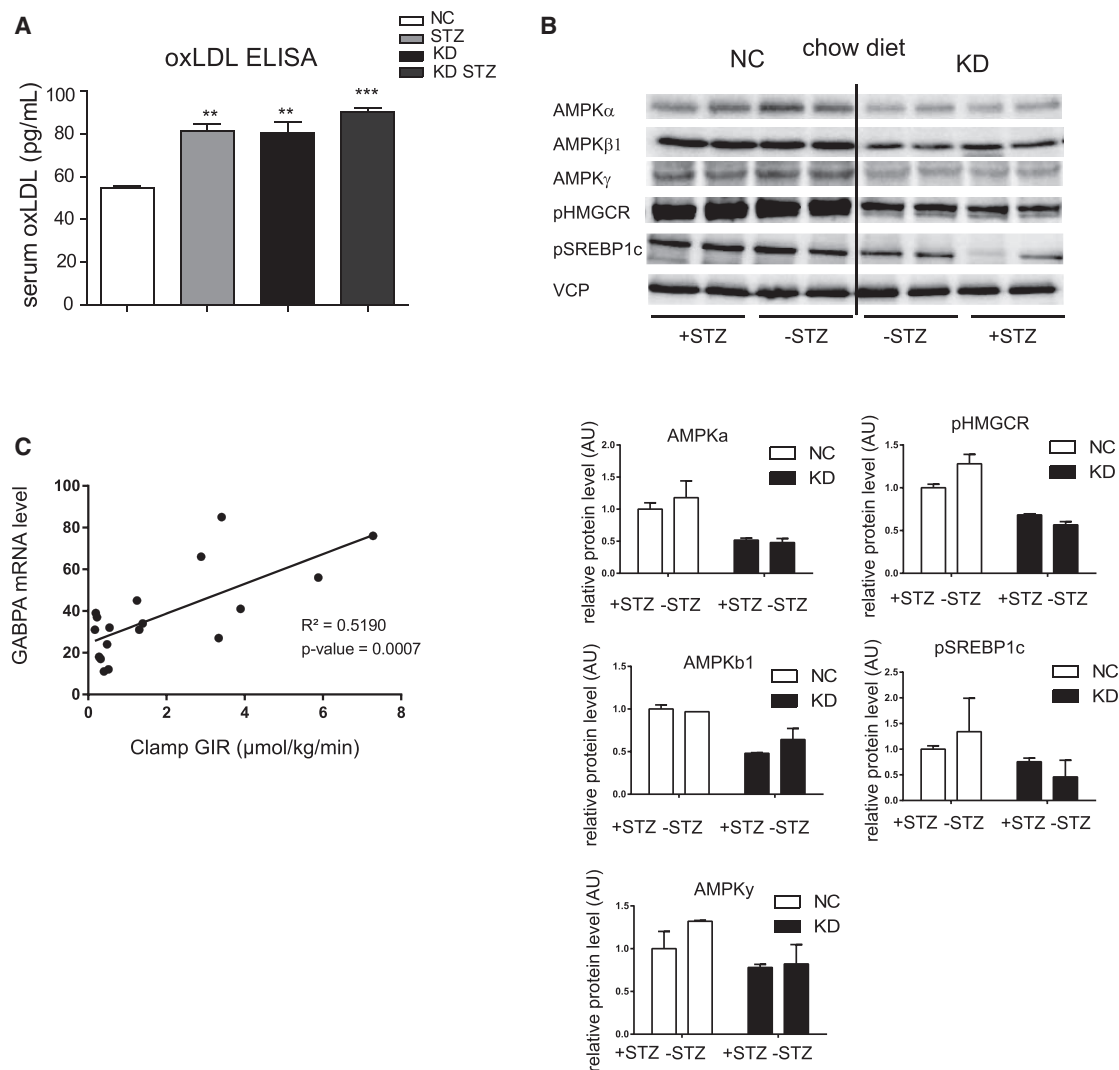
Figure 5. Hepatic Gatekeeper Function of GAbpα

(A) ELISA for oxidized LDL particles in serum of chow fed LDLR-KO mice after STZ treatment and GAbpα knockdown (data are mean ± SEM; **p ≤ 0.01, ***p ≤ 0.001 [relative to NC]; n = 5).

(B) Immunoblots and corresponding densitometric analysis for GAbpα, AMPKβ1, AMPKα, AMPKγ, pHMGCR, and pSREBP1c in liver protein lysates from LDLR-KO mice under chow-fed conditions. VCP served as loading control.

(C) Correlation and p value shown for normalized hepatic GAbpα mRNA levels versus glucose infusion rate (GIR) in a cohort of obese patients (n = 30; Pearson correlation coefficient = 0.7204, p = 0.0007).

See also Figure S5.

the canonical LKB1-dependent activation (Mungai et al., 2011). This is different from the context of the present study, in which elevated ROS levels under chronic inflammatory conditions associated with metabolic disease states and reduced hepatic AMPK activity through decreased hepatic GAbp transcription factor function. This was also reflected by diminished levels of AMPKα, presumably because of destabilization upon disturbed subunit stoichiometry as shown before (Qi et al., 2008), and decreased ACC activation.

Importantly, the role of AMPK as a negative regulator of HMGCoAR activity (Corton and Hardie, 1996; Motoshima et al., 2006), as the rate-limiting enzyme of cholesterol synthesis,

provides an explanation for the observed hypercholesterolemia upon GAbp-dependent reduction in AMPK levels. This is supported by the observed reduction in the levels of the inactive, phosphorylated form of HMGCoAR in GAbpα-deficient livers, suggesting that increased hepatic cholesterol synthesis is responsible for elevated circulating levels.

In congruence with our model, over-activation of HMGCoAR in rat livers was shown in two models of increased ROS production (Pallottini et al., 2005). Similarly, treatment with antioxidants was shown to improve dyslipidemia (Jeong et al., 2012). Consistently, the activity of HMGCoAR correlates with hypercholesterolemia, NAFLD, and cardiovascular risk in patients (Min et al., 2012).

In summary, the present study identifies the dissociation of the GAbp transcriptional complex as a molecular gatekeeper at the interface between inflammation, dyslipidemia, and atherosclerosis. Targeting the anti-atherogenic properties of hepatic GAbp might provide a potential innovative treatment options in diabetic long-term complications.

EXPERIMENTAL PROCEDURES

Cell Culture and Mammalian Two-Hybrid Assay

Hepa1c1 or Hepa1-6 was cultured under standard conditions. Lipofectamine 2000 (Invitrogen) reagent was used for transfection according to the manufacturer's instructions. Cells were treated with recombinant murine TNF-α (BioMol), H_2O_2 (Carl Roth), MnTBAP (Sigma-Aldrich), or NAC (Sigma-Aldrich) for 48 hr. Luciferase assays were performed as previously described (Herzig et al., 2001) using the Bright-Glo luciferase assay system (Promega) and a Mithras plate reader. A constitutive β-galactosidase expression vector (pCVM-betaGal) served as transfection control.

Hepatocyte Isolation and Culturing

Primary hepatocytes were isolated from C57BL/6NHsd male mice via collagenase perfusion as described previously (Zeigerer et al., 2012). Cells were cultured in collagen gel-coated 24-well plates at 200,000 cells/well in Williams E medium (PAN Biotech); substituted with 10% FBS, 100 nM dexamethasone, and penicillin/streptomycin; and maintained at 37°C in an atmosphere with 5% CO_2. After 2 hr of attachment, cultures were washed with PBS and incubated with short hairpin RNA (shRNA) and/or overexpression adenoviruses at a multiplicity of infection (MOI) of 100 or 10, respectively, in Williams E medium for 6 hr. Thereafter cells were washed with PBS and coated with collagen. For H_2O_2 and NAC treatment, primary cells were incubated as indicated 24 hr post-isolation.

Cholesterol Secretion Assay in Primary Hepatocytes

Three days after transduction with knockdown and/or overexpression adenoviruses or GAbpα-specific siRNA (40 nM: SI01008259-Mm_Gabpa_1 FlexiTube siRNA; QIAGEN), primary hepatocytes were washed once with PBS and incubated for 5 hr in serum-free medium containing either no supplements or DMSO as vehicle control for the treatment with 50 μM simvastatin. Cholesterol content in the medium was measured using an Amplex Red Cholesterol Assay Kit (Invitrogen). Cellular protein content was determined for well-based normalization purposes.

Recombinant Viruses

AAVs encoding a GAbpα targeting miRNA (TGC TGT AAA GGT TAG AGC AAA GCT TGG TTT TGG CCA CTG ACT GAC CAA GCT TTT CTA ACC TTT A [termed miRGAbpα]) or a control miRNA (AAA TGT ACT GCG CGT GGA GAC [termed miRNC]) under the control of the hepatocyte-specific LP1 promoter were produced as previously described (Kulozik et al., 2011). For knockdown of GAbpα in primary hepatocytes, recombinant adenoviruses expressing a GAbpα-specific shRNA (5-GGA ACA GAA CAG GAA ACA ATG-3') or a non-specific shRNA (5'-GAT CTG ATC GAC ACT GTA ATG-3') under control of the U6 promoter were cloned as described previously (Lemke et al., 2008). For overexpression in primary hepatocytes as stated above, a previously described constitutively active AMPKα1-expressing adenovirus (Prkaa1^{T172D}) or a GFP-expressing control adenovirus was used (Steinberg et al., 2006).

Animal Experiments

Male 12–16-week-old C57BL/6J, C57BLKS/J, db/db (BKS.Cg-Dock7m $^{2+}$ Lepr^{db}/J), and LDLR-KO (B6.129S7-Ldlr^{tm1Her}/J) mice were obtained from Charles River Laboratories or Jackson Laboratories and maintained on a 12 hr light-dark cycle with regular, unrestricted access to water. For feeding experiments, animals were sacrificed either after a 16 hr fasting or a 16 hr fasting, 6 hr refeeding cycle. C57BL/6J, C57BLKS/J and db/db mice were fed a standard chow diet (D12450B). For in vivo knockdown experiments, 5×10^{11} AAV particles per mouse were administered via tail vein injection. Mice were assigned randomly to the experimental groups. In each experiment,

five to ten animals received identical treatments and were analyzed under fasted, refed, or random fed conditions as indicated. LDLR-KO mice received a chow or a high-cholesterol diet (0.15% cholesterol) for 8 weeks as indicated. Eight weeks after AAV injection, organs and serum were collected, weighed, snap-frozen in liquid N_2, embedded in optimum cutting temperature (OCT) compound, or stored in 4% paraformaldehyde (PFA). STZ (60 mg/g) or vehicle was administered via i.p. injection once daily on 6 consecutive days. Blood glucose levels were monitored, and mice were treated with insulin to maintain serum glucose levels around 400 mg/dl and to prevent mortality. For the TNF-α injection experiment, male C57BL/6J were intravenously (i.v.) injected with 5 μg/kg recombinant human TNF-α (Sigma-Aldrich) and sacrificed 16 hr later.

Animal handling and experimentation were done in accordance with European Union directives and the German Animal Welfare Act and approved by local authorities (Regierungspräsididium Karlsruhe).

Atherosclerotic Lesion Assessment

Aortas were perfused with 0.9% NaCl solution and dissected, fixed in 4% PFA for 2 weeks, and stained with Oil Red O. Aortas were scanned, and fatty streaks were analyzed double blinded and randomized using ImageJ software (NIH).

Blood Metabolites

Serum levels of glucose, total cholesterol, triglycerides (TGs), ketone bodies and non-esterified fatty acids (NEFAs) were determined with the help of an automated glucose monitor (One Touch; Lifescan) or commercially available kits (MP; RANDOX, Crumlin, NIR; WAKO).

Fast Liquid Chromatography

Serum was pooled and subjected to fast liquid chromatography as previously described (Lichtenstein et al., 2007). Cholesterol and TG content was measured in the eluted fractions using commercially available kits as described above.

oxLDL ELISA

oxLDL levels were measured in serum of five mice per experimental group using the commercial ELISA kit SEA527Mu for the detection of oxLDL (USCN).

Tissue Lipid Extraction

Liver lipids were extracted as previously described (Herzig et al., 2003), and TG and total cholesterol content was determined using commercial kits as above. Values were calculated as milligrams per gram wet tissue.

Quantitative Taqman RT-PCR

Total RNA was extracted from pulverized, homogenized mouse liver tissue or primary hepatocytes using Qiazol reagent (QIAGEN) and RNeasy (QIAGEN). cDNA was prepared by reverse transcription using the M-MuLV enzyme and Oligo dT primer. cDNA was amplified using assay-on-demand kits, the ABIPRISM 7700 Sequence detector and the StepOne Plus software. RNA expression data were normalized to levels of TATA-box binding protein (TBP) RNA.

Protein Analysis

Total protein was extracted from fresh or pulverized frozen mouse liver tissue or primary hepatocytes, respectively, using ice-cold cell lysis buffer (50 mM Tris [pH 7.4], 150 mM NaCL, 1% NP-40, 0.5% Triton X-100, 1 mM EDTA, 1 mM Na_3VO_4, 1 mM NaF, 1 μg/mL pepstatin A) with a dounce homogenizer. Twenty micrograms of protein was loaded onto SDS-polyacrylamide gel and blotted onto a nitrocellulose membrane. Western blot assays were performed as previously described (Herzig et al., 2001) using antibodies specific for GABPα (sc-22810), GABPβ (sc-28684) (both from Santa Cruz), pSREBP1c (#9874), AMPKα (#2532), pACC Ser79 (#3661), ACC (#3662), pHSL Ser565 (#4137), HSL (#4107) (all from Cell Signaling), valosin-containing protein (VCP) (ab11433), and AMPKβ1 (ab32112) (both from Abcam), pHMGCR Ser872 (bs-4063R; Bioss Antibodies), GABPβ (H00002553-A01; Abnova), and β-actin (A5441; Sigma-Aldrich). HRP-coupled secondary antibodies were used against mouse IgG and rabbit IgG (Bio-Rad) and goat IgG (Sigma-Aldrich). For detection of multiple proteins in one sample,

nitrocellulose membranes were cut above and below the expected band size and incubated with the respective antibodies. Membranes were stripped with Restore western blot stripping buffer (Thermo Fisher Scientific) and re-incubated with primary antibody. Blots were developed using ECL (RPPN2106; Amersham) or ECL prime (RPN2232; Amersham) and detected with the ChemiDoc imaging system (Bio-Rad). Protein band intensities were determined using the Bio-Rad Image Lab software.

Co-IP

Protein lysate (500 μL; containing 2 mg [liver homogenate] or 1 mg [primary hepatocyte or cell lysate]) were pre-cleared with 40 μl A/G agarose beads (sc-2003; Santa Cruz) for 4 hr. Supernatants were collected and incubated over night with 40 μl protein A/G agarose beads and 5 μg of an antibody specific for GABPβ, mouse IgG, HA antibody, or no antibody. Beads were washed, and proteins were eluted.

ChIP-Seq

Pulverized liver tissue from 12-week-old male C57BL/6 mice was fixed with 1% formaldehyde, and ChIP assays were performed as described (Canettieri et al., 2003) using antibodies specific for GABpα or unspecific IgG (indicated in the Protein Analysis section; both from Santa Cruz). Precipitated DNA fragments were analyzed by sequencing at BGI Europe.

AMPK Activity Assay

AMPK activity was measured in snap-frozen mouse liver tissue with the CycLex AMPK Kinase Assay Kit (#CY-1182; MBL) according to the manufacturer's protocol.

Immunohistochemistry

For Oil Red O lipid staining, 5 μm cryosections of liver embedded in Tissue Tek OCT compound (Sakura) were fixed in Baker's formol. Five-micrometer cryosections of mouse aorta were stained with GAbpa-specific primary antibody (Santa Cruz).

Transcriptome Analysis

MoGene-2_0-st-type from Affymetrix were used. The sense-strand DNA was biotinylated and prepared according the Affymetrix protocol. For gene annotation, CDF Version 17 with Entrez-IDs-based gene definition was used. Resulting raw data were $\log_2$-transformed, quantile-normalized, and corrected for RMA background. Gene expression differences were analyzed using ANOVA with the software SAS JMP7 Genomics version 6 (SAS Institute). A p value of 0.05 with false discovery rate (FDR) correction was regarded as significant. Gene set enrichment analysis (GSEA) was applied for ranked gene list generation, and pathway analysis was performed by KEGG analysis (http://www.genome.jp/kegg/).

Promoter Assay

The following primers were used for amplification of the prkab1 promoter region from genomic mouse DNA (all primer sequences are 5′ to 3′): fw: TTTT GGTCTC AAATTC ACTTGGAGTGAGGTGGTCGGCGCCATC; rv: TTTT GGTCTC TTCGAG GGTCGGACCCCCGGGGATCGCGAGTCAC. The resulting amplicon was digested with BsaI. The whole pFR-Luc plasmid (Agilent) excluding the 5 × Gal4 binding site was PCR-amplified using oligos fw: TTTT CGTCTC CTCGAGTCCGAGCGGAGACTCTAGAG and re: TTTT CGTCTC GAATTCGGTACCCGGTCACAGCTTGTCTG, and the resulting amplicon was digested with BsmBI. The prkab1 promoter and pFR-Luc fragments were ligated, thereby yielding a prkab1 promoter-driven firefly luciferase reporter. HEK293 cells were transfected in 96-well format using Lipofectamine 2000 with the PRKAB1-promoter-reporter pcDNA3.1(-)_Gabpa and pcDNA3.1(-)_Gabpb or the respective amount of pcDNA3.1(-)_empty plasmid and a pCMV-betaGal plasmid for normalization purposes.

Human Studies

GABpα and AMPKβ1 mRNA expression was analyzed in liver tissue samples obtained from 30 extensively characterized Caucasian obese men and women who underwent open abdominal surgery for Roux en Y bypass, sleeve gastrectomy, elective cholecystectomy, or explorative laparotomy. The phenotypic character-ization of the cohort has been extensively described previously (Klöting et al., 2010). Insulin sensitivity was assessed using the euglycemic-hyperinsulinemic clamp method as described previously (Blüher et al., 2002). All baseline blood samples were collected between 8 and 10 a.m. after an overnight fast. All study protocols were approved by the ethics committee of the University of Leipzig (363-10-13122010 and 017-12-230112). All participants gave written informed consent before taking part in the study.

Statistical Analysis

Reported values represent means, and error bars indicate SEM. Statistical analysis was performed using Student's t test for one-factorial designs or two-way ANOVA for multi-factorial studies. p values of 0.05, 0.01, and 0.001 were considered to indicate statistical significance. Analysis was performed using GraphPad Prism (GraphPad Software).

AUTHOR CONTRIBUTIONS

K.N., B.E.U., S.S., M.S., X.W., T.S., Y.F., D.N., M.B., O.S., A.M.G., B.L., K.M.-D., H.-P.H., P.N., T.F., M.D.C., and M.B.D. performed experiments. C.S. and N.G. performed statistical analysis of Affymetrix arrays. M.B. directed clinical research and patient recruitment. A.Z., M.B.D., and S.H. designed and directed the research. M.B.D., K.N., and S.H. wrote the manuscript.

REFERENCES

Akram, M. (2013). A focused review of the role of ketone bodies in health and disease. J. Med. Food 16, 965–967.

Alexandraki, K., Piperi, C., Kalofoutis, C., Singh, J., Alaveras, A., and Kalofoutis, A. (2006). Inflammatory process in type 2 diabetes: the role of cytokines. Ann. N Y Acad. Sci. 1084, 89–117.

Amelio, A.L., Miraglia, L.J., Conkright, J.J., Mercer, B.A., Batalov, S., Cavett, V., Orth, A.P., Busby, J., Hogenesch, J.B., and Conkright, M.D. (2007). A co-activator trap identifies NONO (p54nrb) as a component of the cAMP-signaling pathway. Proc. Natl. Acad. Sci. U S A 104, 20314–20319.

Batchelor, A.H., Piper, D.E., de la Brousse, F.C., McKnight, S.L., and Wolberger, C. (1998). The structure of GABPalpha/beta: an ETS domain-an-kyrin repeat heterodimer bound to DNA. Science 279, 1037–1041.

Blüher, M., Unger, R., Rassoul, F., Richter, V., and Paschke, R. (2002). Relation between glycaemic control, hyperinsulinaemia and plasma concentrations of soluble adhesion molecules in patients with impaired glucose tolerance or Type II diabetes. Diabetologia 45, 210–216.

Cai, D., Yuan, M., Frantz, D.F., Melendez, P.A., Hansen, L., Lee, J., and Shoelson, S.E. (2005). Local and systemic insulin resistance resulting from hepatic activation of IKK-beta and NF-kappaB. Nat. Med. 11, 183–190.

Canettieri, G., Morantte, I., Guzmán, E., Asahara, H., Herzig, S., Anderson, S.D., Yates, J.R., 3rd, and Montminy, M. (2003). Attenuation of a phosphorylation-dependent activator by an HDAC-PP1 complex. Nat. Struct. Biol. 10, 175–181.

Chahil, T.J., and Ginsberg, H.N. (2006). Diabetic dyslipidemia. Endocrinol. Metab. Clin. North Am. 35, 491–510, vii–viii.

Charos, A.E., Reed, B.D., Raha, D., Szekely, A.M., Weissman, S.M., and Snyder, M. (2012). A highly integrated and complex PPARGC1A transcription factor binding network in HepG2 cells. Genome Res. 22, 1668–1679.

Chinenov, Y., Schmidt, T., Yang, X.Y., and Martin, M.E. (1998). Identification of redox-sensitive cysteines in GA-binding protein-alpha that regulate DNA binding and heterodimerization. J. Biol. Chem. 273, 6203–6209.

Chinenov, Y., Henzl, M., and Martin, M.E. (2000). The alpha and beta subunits of the GA-binding protein form a stable heterodimer in solution. Revised model of heterotetrameric complex assembly. J. Biol. Chem. 275, 7749–7756.

Corton, J.M., and Hardie, D.G. (1996). Regulation of lipid biosynthesis by the AMP-activated protein kinase and its role in the hepatocellular response to stress. Prog. Liver Dis. 14, 69–99.

Coughlan, K.A., Valentine, R.J., Ruderman, N.B., and Saha, A.K. (2014). AMPK activation: a therapeutic target for type 2 diabetes? Diabetes Metab. Syndr. Obes. 7, 241–253.

Emerling, B.M., Weinberg, F., Snyder, C., Burgess, Z., Mutlu, G.M., Viollet, B., Budinger, G.R., and Chandel, N.S. (2009). Hypoxic activation of AMPK is dependent on mitochondrial ROS but independent of an increase in AMP/ATP ratio. Free Radic. Biol. Med. 46, 1386–1391.

Fromm, L., and Burden, S.J. (2001). Neuregulin-1-stimulated phosphorylation of GABP in skeletal muscle cells. Biochemistry 40, 5306–5312.

Geier, A., Dietrich, C.G., Voigt, S., Ananthanarayanan, M., Lammert, F., Schmitz, A., Trauner, M., Wasmuth, H.E., Boraschi, D., Balasubramaniyan, N., et al. (2005). Cytokine-dependent regulation of hepatic organic anion transporter gene transactivators in mouse liver. Am. J. Physiol. Gastrointest. Liver Physiol. 289, G831–G841.

Goldberg, I.J., Hu, Y., Noh, H.L., Wei, J., Huggins, L.A., Rackmill, M.G., Hamai, H., Reid, B.N., Blaner, W.S., and Huang, L.S. (2008). Decreased lipoprotein clearance is responsible for increased cholesterol in LDL receptor knockout mice with streptozotocin-induced diabetes. Diabetes 57, 1674–1682.

Gregor, M.F., and Hotamisligil, G.S. (2011). Inflammatory mechanisms in obesity. Annu. Rev. Immunol. 29, 415–445.

Hardie, D.G. (2013). AMPK: a target for drugs and natural products with effects on both diabetes and cancer. Diabetes 62, 2164–2172.

Hardie, D.G. (2014). AMPK—sensing energy while talking to other signaling pathways. Cell Metab. 20, 939–952.

Herzig, S., Long, F., Jhala, U.S., Hedrick, S., Quinn, R., Bauer, A., Rudolph, D., Schutz, G., Yoon, C., Puigserver, P., et al. (2001). CREB regulates hepatic gluconeogenesis through the coactivator PGC-1. Nature 413, 179–183.

Herzig, S., Hedrick, S., Morantte, I., Koo, S.H., Galimi, F., and Montminy, M. (2003). CREB controls hepatic lipid metabolism through nuclear hormone receptor PPAR-gamma. Nature 426, 190–193.

Houstis, N., Rosen, E.D., and Lander, E.S. (2006). Reactive oxygen species have a causal role in multiple forms of insulin resistance. Nature 440, 944–948.

Ishibashi, S., Goldstein, J.L., Brown, M.S., Herz, J., and Burns, D.K. (1994). Massive xanthomatosis and atherosclerosis in cholesterol-fed low density lipoprotein receptor-negative mice. J. Clin. Invest. 93, 1885–1893.

Jeong, S.M., Kang, M.J., Choi, H.N., Kim, J.H., and Kim, J.I. (2012). Quercetin ameliorates hyperglycemia and dyslipidemia and improves antioxidant status in type 2 diabetic db/db mice. Nutr. Res. Pract. 6, 201–207.

Kalofoutis, C., Piperi, C., Kalofoutis, A., Harris, F., Phoenix, D., and Singh, J. (2007). Type II diabetes mellitus and cardiovascular risk factors: current therapeutic approaches. Exp. Clin. Cardiol. 12, 17–28.

Keren, P., George, J., Shaish, A., Levkovitz, H., Janakovic, Z., Afek, A., Goldberg, I., Kopolovic, J., Keren, G., and Harats, D. (2000). Effect of hyperglycemia and hyperlipidemia on atherosclerosis in LDL receptor-deficient mice: establishment of a combined model and association with heat shock protein 65 immunity. Diabetes 49, 1064–1069.

Klop, B., Elte, J.W., and Cabezas, M.C. (2013). Dyslipidemia in obesity: mechanisms and potential targets. Nutrients 5, 1218–1240.

Klöting, N., Fasshauer, M., Dietrich, A., Kovacs, P., Schön, M.R., Kern, M., Stumvoll, M., and Blüher, M. (2010). Insulin-sensitive obesity. Am. J. Physiol. Endocrinol. Metab. 299, E506–E515.

Kulozik, P., Jones, A., Mattijssen, F., Rose, A.J., Reimann, A., Strzoda, D., Kleinsorg, S., Raupp, C., Kleinschmidt, J., Müller-Decker, K., et al. (2011). Hepatic deficiency in transcriptional cofactor TBL1 promotes liver steatosis and hypertriglyceridemia. Cell Metab. 13, 389–400.

Kunjathoor, V.V., Wilson, D.L., and LeBoeuf, R.C. (1996). Increased atherosclerosis in streptozotocin-induced diabetic mice. J. Clin. Invest. 97, 1767–1773.

Lemke, U., Krones-Herzig, A., Berriel Diaz, M., Narvekar, P., Ziegler, A., Vegiopoulos, A., Cato, A.C., Bohl, S., Klingmüller, U., Screaton, R.A., et al. (2008). The glucocorticoid receptor controls hepatic dyslipidemia through Hes1. Cell Metab. 8, 212–223.

Li, Q., Spencer, N.Y., Oakley, F.D., Buettner, G.R., and Engelhardt, J.F. (2009). Endosomal Nox2 facilitates redox-dependent induction of NF-kappaB by TNF-alpha. Antioxid. Redox Signal. 11, 1249–1263.

Li, Y., Xu, S., Mihaylova, M.M., Zheng, B., Hou, X., Jiang, B., Park, O., Luo, Z., Lefai, E., Shyy, J.Y., et al. (2011). AMPK phosphorylates and inhibits SREBP activity to attenuate hepatic steatosis and atherosclerosis in diet-induced insulin-resistant mice. Cell Metab. 13, 376–388.

Lichtenstein, L., Berbée, J.F., van Dijk, S.J., van Dijk, K.W., Bensadoun, A., Kema, I.P., Voshol, P.J., Müller, M., Rensen, P.C., and Kersten, S. (2007). Angptl4 upregulates cholesterol synthesis in liver via inhibition of LPL- and HL-dependent hepatic cholesterol uptake. Arterioscler Thromb Vasc Biol. 27, 2420–2427.

Mariappan, N., Elks, C.M., Sriramula, S., Guggilam, A., Liu, Z., Borkhsenious, O., and Francis, J. (2010). NF-kappaB-induced oxidative stress contributes to mitochondrial and cardiac dysfunction in type II diabetes. Cardiovasc. Res. 85, 473–483.

Martin, M.E., Chinenov, Y., Yu, M., Schmidt, T.K., and Yang, X.Y. (1996). Redox regulation of GA-binding protein-alpha DNA binding activity. J. Biol. Chem. 271, 25617–25623.

Mathé, D. (1995). Dyslipidemia and diabetes: animal models. Diabete Metab. 21, 106–111.

Michael, M.D., Kulkarni, R.N., Postic, C., Previs, S.F., Shulman, G.I., Magnuson, M.A., and Kahn, C.R. (2000). Loss of insulin signaling in hepatocytes leads to severe insulin resistance and progressive hepatic dysfunction. Mol. Cell 6, 87–97.

Min, H.K., Kapoor, A., Fuchs, M., Mirshahi, F., Zhou, H., Maher, J., Kellum, J., Warnick, R., Contos, M.J., and Sanyal, A.J. (2012). Increased hepatic synthesis and dysregulation of cholesterol metabolism is associated with the severity of nonalcoholic fatty liver disease. Cell Metab. 15, 665–674.

Miyazaki, Y., Pipek, R., Mandarino, L.J., and DeFronzo, R.A. (2003). Tumor necrosis factor alpha and insulin resistance in obese type 2 diabetic patients. Int. J. Obes. Relat. Metab. Disord. 27, 88–94.

Motoshima, H., Goldstein, B.J., Igata, M., and Araki, E. (2006). AMPK and cell proliferation–AMPK as a therapeutic target for atherosclerosis and cancer. J. Physiol. 574, 63–71.

Mungai, P.T., Waypa, G.B., Jairaman, A., Prakriya, M., Dokic, D., Ball, M.K., and Schumacker, P.T. (2011). Hypoxia triggers AMPK activation through reactive oxygen species-mediated activation of calcium release-activated calcium channels. Mol. Cell. Biol. *31*, 3531–3545.

O'Neill, L.A., and Hardie, D.G. (2013). Metabolism of inflammation limited by AMPK and pseudo-starvation. Nature *493*, 346–355.

Oliff, A., Defeo-Jones, D., Boyer, M., Martinez, D., Kiefer, D., Vuocolo, G., Wolfe, A., and Socher, S.H. (1987). Tumors secreting human TNF/cachectin induce cachexia in mice. Cell *50*, 555–563.

Pallottini, V., Martini, C., Pascolini, A., Cavallini, G., Gori, Z., Bergamini, E., Incerpi, S., and Trentalance, A. (2005). 3-Hydroxy-3-methylglutaryl coenzyme A reductase deregulation and age-related hypercholesterolemia: a new role for ROS. Mech. Ageing Dev. *126*, 845–851.

Panchal, S.K., and Brown, L. (2011). Rodent models for metabolic syndrome research. J. Biomed. Biotechnol. *2011*, 351982.

Qi, J., Gong, J., Zhao, T., Zhao, J., Lam, P., Ye, J., Li, J.Z., Wu, J., Zhou, H.M., and Li, P. (2008). Downregulation of AMP-activated protein kinase by Cidea-mediated ubiquitination and degradation in brown adipose tissue. EMBO J. *27*, 1537–1548.

Rosmarin, A.G., Resendes, K.K., Yang, Z., McMillan, J.N., and Fleming, S.L. (2004). GA-binding protein transcription factor: a review of GABP as an integrator of intracellular signaling and protein-protein interactions. Blood Cells Mol. Dis. *32*, 143–154.

Ryu, D., Jo, Y.S., Lo Sasso, G., Stein, S., Zhang, H., Perino, A., Lee, J.U., Zeviani, M., Romand, R., Hottiger, M.O., et al. (2014). A SIRT7-dependent acetylation switch of GABPβ1 controls mitochondrial function. Cell Metab. *20*, 856–869.

Shoelson, S.E., Herrero, L., and Naaz, A. (2007). Obesity, inflammation, and insulin resistance. Gastroenterology *132*, 2169–2180.

Steinberg, G.R., Michell, B.J., van Denderen, B.J., Watt, M.J., Carey, A.L., Fam, B.C., Andrikopoulos, S., Proietto, J., Görgün, C.Z., Carling, D., et al. (2006). Tumor necrosis factor alpha-induced skeletal muscle insulin resistance involves suppression of AMP-kinase signaling. Cell Metab. *4*, 465–474.

Sunesen, M., Huchet-Dymanus, M., Christensen, M.O., and Changeux, J.P. (2003). Phosphorylation-elicited quaternary changes of GA binding protein in transcriptional activation. Mol. Cell. Biol. *23*, 8008–8018.

Turner, N., Kowalski, G.M., Leslie, S.J., Risis, S., Yang, C., Lee-Young, R.S., Babb, J.R., Meikle, P.J., Lancaster, G.I., Henstridge, D.C., et al. (2013). Distinct patterns of tissue-specific lipid accumulation during the induction of insulin resistance in mice by high-fat feeding. Diabetologia *56*, 1638–1648.

Uysal, K.T., Wiesbrock, S.M., Marino, M.W., and Hotamisligil, G.S. (1997). Protection from obesity-induced insulin resistance in mice lacking TNF-alpha function. Nature *389*, 610–614.

Uysal, K.T., Wiesbrock, S.M., and Hotamisligil, G.S. (1998). Functional analysis of tumor necrosis factor (TNF) receptors in TNF-alpha-mediated insulin resistance in genetic obesity. Endocrinology *139*, 4832–4838.

Vikramadithyan, R.K., Hu, Y., Noh, H.L., Liang, C.P., Hallam, K., Tall, A.R., Ramasamy, R., and Goldberg, I.J. (2005). Human aldose reductase expression accelerates diabetic atherosclerosis in transgenic mice. J. Clin. Invest. *115*, 2434–2443.

Viollet, B., Mounier, R., Leclerc, J., Yazigi, A., Foretz, M., and Andreelli, F. (2007). Targeting AMP-activated protein kinase as a novel therapeutic approach for the treatment of metabolic disorders. Diabetes Metab. *33*, 395–402.

Viollet, B., Guigas, B., Leclerc, J., Hébrard, S., Lantier, L., Mounier, R., Andreelli, F., and Foretz, M. (2009). AMP-activated protein kinase in the regulation of hepatic energy metabolism: from physiology to therapeutic perspectives. Acta Physiol. (Oxf.) *196*, 81–98.

Wallerman, O., Motallebipour, M., Enroth, S., Patra, K., Bysani, M.S., Komorowski, J., and Wadelius, C. (2009). Molecular interactions between HNF4a, FOXA2 and GABP identified at regulatory DNA elements through ChIP-sequencing. Nucleic Acids Res. *37*, 7498–7508.

Wu, H., Xiao, Y., Zhang, S., Ji, S., Wei, L., Fan, F., Geng, J., Tian, J., Sun, X., Qin, F., et al. (2013). The Ets transcription factor GABP is a component of the hippo pathway essential for growth and antioxidant defense. Cell Rep. *3*, 1663–1677.

Yamakawa, T., Tanaka, S., Yamakawa, Y., Kiuchi, Y., Isoda, F., Kawamoto, S., Okuda, K., and Sekihara, H. (1995). Augmented production of tumor necrosis factor-alpha in obese mice. Clin. Immunol. Immunopathol. *75*, 51–56.

Zeigerer, A., Gilleron, J., Bogorad, R.L., Marsico, G., Nonaka, H., Seifert, S., Epstein-Barash, H., Kuchimanchi, S., Peng, C.G., Ruda, V.M., et al. (2012). Rab5 is necessary for the biogenesis of the endolysosomal system in vivo. Nature *485*, 465–470.

Zschiedrich, I., Hardeland, U., Krones-Herzig, A., Berriel Diaz, M., Vegiopoulos, A., Müggenburg, J., Sombroek, D., Hofmann, T.G., Zawatzky, R., Yu, X., et al. (2008). Coactivator function of RIP140 for NFkappaB/RelA-dependent cytokine gene expression. Blood *112*, 264–276.